Journal of Physics:
Conference Series

PAPER • **OPEN ACCESS**

Filament instability under constant loads

To cite this article: A. G. Monastra *et al* 2018 *J. Phys.: Conf. Ser.* **1012** 012010

IOP Conf. Series: Journal of Physics: Conf. Series **1012** (2018) 012010 doi:10.1088/1742-6596/1012/1/012010

Filament instability under constant loads

A. G. Monastra[1,4,*], M. F. Carusela[1,4], M. V. D'Angelo[2,4] and L. Bruno[3,4]

[1] Instituto de Ciencias, Universidad Nacional de Gral. Sarmiento, Los Polvorines, Buenos Aires, Argentina
[2] Grupo de Medios Porosos, Facultad de Ingeniería , Universidad Nacional de Buenos Aires, Argentina
[3] Departamento de Física & IFIBA-CONICET, Facultad de Ciencias Exactas y Naturales, Universidad Nacional de Buenos Aires, Argentina
[4] Consejo Nacional de Investigaciones Científicas y Técnicas, Argentina

E-mail: *amonast@ungs.edu.ar

Abstract. Buckling of semi-flexible filaments appears in different systems and scales. Some examples are: fibers in geophysical applications, microtubules in the cytoplasm of eukaryotic cells and deformation of polymers freely suspended in a flow. In these examples, instabilities arise when a system's parameter exceeds a critical value, being the Euler force the most known. However, the complete time evolution and wavelength of buckling processes are not fully understood. In this work we solve analytically the time evolution of a filament under a constant compressive force in the small amplitude approximation. This gives an insight into the variable force scenario in terms of normal modes. The evolution is highly sensitive to the initial configuration and to the magnitude of the compressive load. This model can be a suitable approach to many different real situations.

1. Introduction

The beam theory stablishes that when a compressive force is applied to the end of a slender rod, it collapses and buckles when the force exceeds a critical value [1, 2]. The shape of the buckled filament depends on the boundary conditions. The Euler force depends on the rod geometry and its elasticity. For a clamped-clamped filament its value is:

$$P_c = 4\pi^2 \frac{EI}{L^2} \ , \tag{1}$$

where E, I and L are the filament's Young modulus, the second moment of inertia and length, respectively. Importantly, the critical force does not depend on the environment where the buckling takes place. However, the way the buckling proceeds after the critical force is surpassed (e.g. the characteristic time taken for the filament to achieve a stationary shape) does strongly depend on the surrounding viscosity [3]. In Fig. 1 a slender filament immersed in glycerol compressed under two different loads is shown. For forces slightly larger that the Euler one the filament displays a sinusoidal shape with a characteristic wavelength of the order of its length. On the other hand, if the load largely exceeds the critical value, the filament deforms more rapidly and with a shorter wavelength.

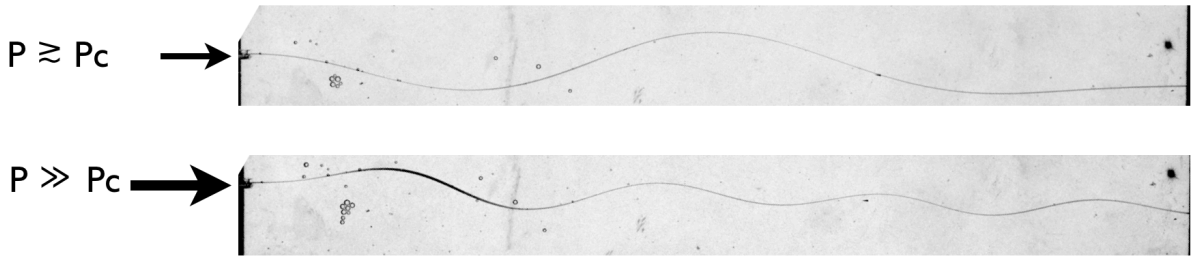

Figure 1. Snapshots of a compressing polyethylene terephthalate filament in glycerol for two different values of the applied force. The length of the filament is 30 cm.

Deformation of flexible fibers is of interest in areas such as physics, biology or engineering, and in view of their potential applications in many different industrial fields. Examples include the manufacturing of fiber-reinforced composites [4, 5], the rheology of biological polymers [6], and the motility of microorganisms [7, 8]. The use of long optical fibers has been suggested as a method to realize distributed in situ measurements (temperature for instance) on natural water flows [9]. Also fibers are widely used by petroleum engineers [10] to enhance the proppant transport capabilities of fracturing fluids, or to prevent the backflow of proppant. Other domains of application are civil engineering (special cements, structural reinforcement), textile engineering, bio engineering and medicine.

In this work we develop an general description of the behaviour of filaments immersed in a viscous medium under compression in terms of normal modes. Our approach intends to explore a general phenomenon that can be found in a variety of micro to macro scales systems and applications.

2. Theoretical approach

The shape of a semi-flexible filament is determined by the position of its neutral axis $\mathbf{r}(l)$, with l a curvilinear coordinate along the filament varying from 0 to L. This configuration has an elastic energy due to strain ε given by:

$$V_{\mathrm{E}} = \frac{1}{2}EA\int_0^L \varepsilon^2(l)\mathrm{d}l = \frac{1}{2}EA\int_0^L (|\mathbf{r}'(l)|-1)^2\mathrm{d}l \ , \tag{2}$$

where A is the transversal area of the filament. Also, the filament has a bending energy given by its curvature $\mathcal{C}$:

$$V_{\mathrm{B}} = \frac{1}{2}EI\int_0^L \mathcal{C}^2(l)(1+\varepsilon(l))^2\mathrm{d}l = \frac{1}{2}EI\int_0^L \frac{|\mathbf{r}'(l)\times\mathbf{r}''(l)|^2}{|\mathbf{r}'(l)|^4}\mathrm{d}l \ . \tag{3}$$

In both formulas the primes indicate derivative with respect to the coordinate l. Applying a Lagrangian minimization principle, one can compute the forces on an infinitesimal segment $\mathrm{d}l$ at position l due to strain (elastic force $\mathbf{f}_{\mathrm{E}}$) and curvature (bending force $\mathbf{f}_{\mathrm{B}}$), which are produced by the neighbouring segments. The full expressions are rather complicate, involving up to the fourth derivative of the position $\mathbf{r}(l)$.

Since the filament is immersed in an homogeneous viscous medium, we consider the viscous drag on a filament element as $\mathbf{f}_{\mathrm{V}} = -c\dot{\mathbf{r}}$. In this expression c is the drag coefficient per unit length, which is proportional to the dynamical viscosity, and the dot accounts for time derivative.

In an overdamped regime, the inertia term can be neglected and the equation of motion for an infinitesimal segment is given by:

$$\mathbf{f}_{\mathrm{E}} + \mathbf{f}_{\mathrm{B}} + \mathbf{f}_{\mathrm{V}} = 0 \ . \tag{4}$$

If the filament motion is constrained to two dimensions, its shape can be parametrized as:

$$\mathbf{r}(l) = (l + \delta x(l); \delta y(l); 0) \ , \tag{5}$$

and we consider a small amplitude approximation $\delta x, \delta y \ll L$.

Replacing this parametrization in Eq. (4), it can be shown that $\delta x''$ and higher order derivatives are proportional to second order derivatives of δy. Moreover, the time derivative $\delta \dot{x}$ is exponentially small after a short initial time τ_{E} given by

$$\tau_{\mathrm{E}} = \frac{c}{EA} \left(\frac{L}{\pi} \right)^2 \ . \tag{6}$$

Also, when the filament is under a compressive load P, at first order we obtain for the strain

$$\delta x'(l) = -\frac{P}{EA} \ , \tag{7}$$

which is usually much smaller than one. Taking into account this result, the amplitude in the transversal direction δy is determined by the following equation:

$$\left(1 + \frac{2P}{EA} \right) EI \delta y'''' + P \delta y'' + c_{\perp} \delta \dot{y} = 0 \ . \tag{8}$$

This is the so called hydrodinamic equation [3]. To solve this linear differential equation, we propose separation of variables and exponential dependence:

$$\delta y(l, t) = \mathcal{C} \exp(kl) \exp(\Gamma t) \ . \tag{9}$$

Replacing this proposed solution into Eq. (8) we obtain

$$\left(1 + \frac{2P}{EA} \right) EI k^4 + P k^2 + c\Gamma = 0 \ . \tag{10}$$

This is a fourth order polynomial in k which gives four possible solutions which can be superposed. It is convenient to redefine the parameters as:

$$p = \frac{L^2 P}{\left(1 + \frac{2P}{EA} \right) EI} \ , \tag{11}$$

$$\gamma = \frac{c L^4 \Gamma}{\left(1 + \frac{2P}{EA} \right) EI} = \tau_{\mathrm{B}} \Gamma \ , \tag{12}$$

$$\kappa = kL \ . \tag{13}$$

The value p corresponds to a dimensionless compressing load and γ is the dimensionless decaying/growing rate, whose natural scale is a characteristic *bending* time τ_{B}, which is much bigger than τ_{E} for a slender filament. In terms of these dimensionless parameters the characteristic polynomial can be written as:

$$\kappa^4 + p\kappa^2 + \gamma = 0 \ . \tag{14}$$

For $\gamma < 0$, which corresponds to a decreasing solution in time, the four possible solutions are $\kappa = \{\mathrm{i}\kappa_1; -\mathrm{i}\kappa_1; \kappa_2; -\kappa_2\}$, with

$$\kappa_1 = \sqrt{\frac{\sqrt{p^2 - 4\gamma} + p}{2}} , \tag{15}$$

$$\kappa_2 = \sqrt{\frac{\sqrt{p^2 - 4\gamma} - p}{2}} . \tag{16}$$

Therefore in this case the general solution can be written as a superposition of circular and hyperbolic trigonometric functions.

For $0 < \gamma < p^2/4$, the amplitude grows exponentially, and there are four possible pure imaginary solutions $\kappa = \{\mathrm{i}\kappa_1; -\mathrm{i}\kappa_1; \mathrm{i}\kappa_3; -\mathrm{i}\kappa_3\}$, with κ_1 as in Eq. (15), and

$$\kappa_3 = \sqrt{\frac{p - \sqrt{p^2 - 4\gamma}}{2}} . \tag{17}$$

These solutions can be written as circular trigonometric solutions. For $\gamma > p^2/4$ the four possible values of κ are complex. Nevertheless, it turns out that these solutions do not arise for the boundary conditions that we study. The general solutions can be written as

$$\delta y(l,t) = [\mathcal{C}_1 \cos(\kappa_1 l/L) + \mathcal{D}_1 \sin(\kappa_1 l/L) + \mathcal{C}_2 \cosh(\kappa_2 l/L) + \mathcal{D}_2 \sinh(\kappa_2 l/L)] \exp(\gamma t/\tau_\mathrm{B}), \tag{18}$$

$$\delta y(l,t) = [\mathcal{C}_1 \cos(\kappa_1 l/L) + \mathcal{D}_1 \sin(\kappa_1 l/L) + \mathcal{C}_3 \cos(\kappa_3 l/L) + \mathcal{D}_3 \sin(\kappa_3 l/L)] \exp(\gamma t/\tau_\mathrm{B}), \tag{19}$$

for negative and positive γ, respectively. The constants $\mathcal{C}_i$ and $\mathcal{D}_i$ should be much smaller than L to fulfill the small deformation approximation, and in the case of a growing solution with $\gamma > 0$, it will only be valid for a time such that $\mathcal{C}_i \exp(\gamma t/\tau_\mathrm{B}) \ll L$.

We are particularly interested in the clamped-clamped boundary condition, as shown in Fig. 1, where both ends remain horizontal, and always at the same vertical position. Due to the symmetry of these boundary conditions, it is more convenient to shift the coordinate l, going from $-L/2$ to $L/2$. Therefore the clamped-clamped boundary condition corresponds to $\delta y(\pm L/2, t) = 0$ and $\delta y'(\pm L/2, t) = 0$. These four conditions provide us four equations to determine the constants $\mathcal{C}_i$ and $\mathcal{D}_i$. Moreover, with simple sums and substractions of the equations, they decouple to

$$\mathcal{C}_1 \cos(\kappa_1/2) + \mathcal{C}_2 \cosh(\kappa_2/2) = 0 , \tag{20}$$

$$-\mathcal{C}_1 \kappa_1 \sin(\kappa_1/2) + \mathcal{C}_2 \kappa_2 \sinh(\kappa_2/2) = 0 , \tag{21}$$

$$\mathcal{D}_1 \sin(\kappa_1/2) + \mathcal{D}_2 \sinh(\kappa_2/2) = 0 , \tag{22}$$

$$\mathcal{D}_1 \kappa_1 \cos(\kappa_1/2) + \mathcal{D}_2 \kappa_2 \cosh(\kappa_2/2) = 0 . \tag{23}$$

The first two equations determine symmetric solutions, while the last two antisymmetric ones. In order to avoid the trivial solution, the determinant for each pair of equations should be zero. For $\gamma < 0$:

$$\mathcal{J}^{(+)}(p,\gamma) = \kappa_2 \sinh(\kappa_2/2) \cos(\kappa_1/2) + \kappa_1 \sin(\kappa_1/2) \cosh(\kappa_2/2) , \tag{24}$$

$$\mathcal{J}^{(-)}(p,\gamma) = \kappa_2 \cosh(\kappa_2/2) \sin(\kappa_1/2) - \kappa_1 \cos(\kappa_1/2) \sinh(\kappa_2/2) . \tag{25}$$

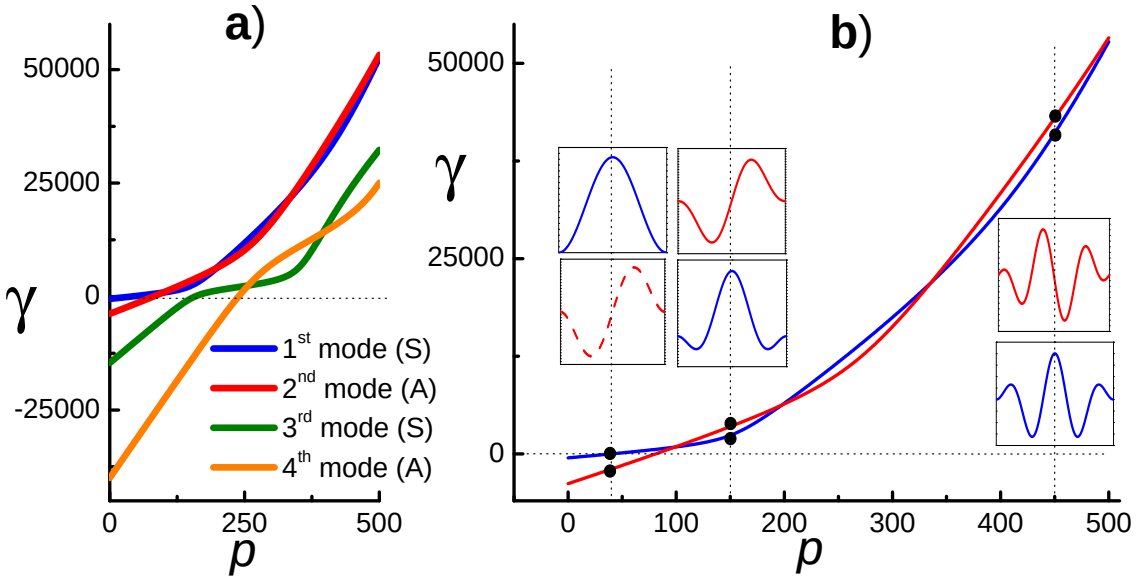

Figure 2. (a) Plot of dimensionless characteristic rates γ versus compressive force p for the first symmetric (S) and antisymmetric (A) modes. (b) Detail for the first symmetric and antisymmetric modes. The insets display the filament shapes for $p = 40, 150$ and 450. Dashed line represents a mode with a decaying amplitude.

We can proceed in the same way for the case $0 < \gamma < p^2/4$, and the determinants are:

$$\mathcal{J}^{(+)}(p,\gamma) = \kappa_3 \sin(\kappa_3/2)\cos(\kappa_1/2) - \kappa_1 \sin(\kappa_1/2)\cos(\kappa_2/2) \ , \quad (26)$$

$$\mathcal{J}^{(-)}(p,\gamma) = \kappa_3 \cos(\kappa_3/2)\sin(\kappa_1/2) - \kappa_1 \cos(\kappa_1/2)\sin(\kappa_3/2) \ . \quad (27)$$

The dimensionless parameter p is determined using Eq. (11). The values of γ that vanish the corresponding determinants, provide *quantized* hydrodynamic modes.

We plot these quantized values of γ as a function of the parameter p in Fig. 2 for the first four modes (those with the highest value of γ). For $p < 4\pi^2$ all modes have a negative value of γ, corresponding to a compressive force smaller than the critical value. As this value is surpassed, there are growing modes which contribute to the buckling process, being the first two the fastest ones. We also observe an interesting successive crossovers between the symmetric and antisymmetric modes. This implies that for some range of compressing force p, the antisymmetric mode grows faster than the symmetric one, and for other ranges the opposite situation is observed (see Fig. 2).

The shape of the different modes, for decaying rates $\gamma < 0$ are:

$$\Psi_n^{(+)}(p,u) = \mathcal{K}_n \left[\cosh(\kappa_2/2)\cos(\kappa_1 u) - \cos(\kappa_1/2)\cosh(\kappa_2 u)\right] \ , \quad (28)$$

$$\Psi_n^{(-)}(p,u) = \mathcal{K}_n \left[\sinh(\kappa_2/2)\sin(\kappa_1 u) - \sin(\kappa_1/2)\sinh(\kappa_2 u)\right] \ , \quad (29)$$

corresponding to symmetric and antisymmetric modes, respectively. The dimensionless coordinate along the filament $u = l/L$ ranges from -1/2 to 1/2. For growing rates $\gamma > 0$ the filament shapes are:

$$\Psi_n^{(+)}(p,u) = \mathcal{K}_n \left[\cos(\kappa_3/2)\cos(\kappa_1 u) - \cos(\kappa_1/2)\cos(\kappa_3 u)\right] , \quad (30)$$

$$\Psi_n^{(-)}(p,u) = \mathcal{K}_n \left[\sin(\kappa_3/2)\sin(\kappa_1 u) - \sin(\kappa_1/2)\sin(\kappa_3 u)\right] . \quad (31)$$

These modes depend parametrically on the compressive force. For a given value of p, the different possible discretized values of γ determine the corresponding values of κ_1 and κ_2 (or κ_3 if $\gamma > 0$) through Eqs. (15), (16) and (17). For a convenient choice of the arbitrary constants $\mathcal{K}_n$, the different modes are orthonormal, fulfilling

$$\int_{-1/2}^{1/2} \Psi_n(p,u)\Psi_m(p,u)\mathrm{d}u = \delta_{nm} \quad (32)$$

The general solution for a constant compressing load P is

$$\delta y(l,t) = \sum_{n=1}^{\infty} a_n \Psi_n(p, l/L)\exp(\gamma_n t/\tau_\mathrm{B}) \quad (33)$$

where the coefficients a_n are determined from the initial condition of the filament projected on each eigenmode. As an example, in Fig. 2 (b), we plot the shape of the first two modes. We observe that as the parameter p increases, the modes have more nodes and the typical wavelengths are shorter. This situation describes the experimental behaviour observed in Fig. 1.

3. Conclusions

In this paper we have explored the buckling dynamics of a semi-flexible filament immersed in a viscous environment. We have found analytical solutions of the hydrodynamics beam equation in the small deformation limit in terms of hydrodynamics modes. These modes have characteristic relaxation times and critical forces, which depend on geometrical and mechanical parameters of the filament, the medium viscosity and the magnitude of the compression. When the compression load is very small, the filament shape straightens. However, if the compression magnitude surpassed a critical value, an interesting scenario occurs: the buckling shape will depend on the magnitude of the compression. Moreover, successive crossovers between symmetric and antisymmetric modes are observed, depending on the particular value of the compressive load.

These results show that the shape of a filament under compression is more complex than that of a single sinusoidal mode. This work provides a theoretical explanation that can help to understand the evolution of filament buckling when a variable force is applied, which it is the case in most experiments. The spatio-temporal characterization of the buckling can have significant importance in many field applications where a flexible filament is dramatically compressed within a viscous environment.

Acknowledgments

All authors are members of CIC-CONICET. AGM and MFC want to thank for the funding project PIO-CONICET-UNGS.

References

[1] Landau L D and Lifshitz E M 1986 *Theory of Elasticity*, vol 7, Course of Theoretical Physics (New York: Elsevier)
[2] Timoshenko S P and Gere J M 1963 *Theory of Elastic Stability* (New York: McGraw-Hill Book Company)
[3] Howard J 2001 *Mechanics of motor proteins and the cytoskeleton* (Sunderland, MA: Sinauer Associates, Publishers)
[4] Yasuda K, Mori N and Nakamura K 2002 A new visualization technique for short fibers in a slit flow of fiber suspensions *International Journal of Engineering Science* **40** 1037-1052

[5] Yoo DY, Kim S, Park GJ, Park JJ and Kim SW 2017 Effects of fiber shape, aspect ratio, and volume fraction on flexural behavior of ultra-high-performance fiber-reinforced cement composites *Composite Structures* **174** 375-388
[6] Lagomarsino M, Pagonabarraga I and Lowe C 2005 Hydrodynamic induced deformation and orientation of a microscopic elastic filament *Phys. Rev. Lett.* **94** 148104
[7] Lowe C 2003 Dynamics of filaments: modelling the dynamics of driven microfilaments *Philos. Trans. R. Soc. London* B **358** 1543-1550
[8] Chaban B, Velocity Hughes H and Beeby M 2015 The flagellum in bacterial pathogens: For motility and a whole lot more *Seminars in Cell & Developmental Biology* **46** 91-103
[9] Selker J, van de Giesen M, Westhoff N, Luxemburg W and Parlange MB 2006 Fiber optics opens window on stream dynamics *Geophys. Res. Lett.* **33** L24401
[10] Howard PR, King MT, Morris M, Feraud JP, Slusher G and Lipari S 1995 Fiber/proppant mixtures control proppant flowback in South Texas *SPE Annual Technical Conference and Exhibition* (Dallas, TX: Society of Petroleum Engineers) pp 453-454